Case Studies in Thermal Engineering 43 (2023) 102816

Contents lists available at ScienceDirect

Case Studies in Thermal Engineering

journal homepage: www.elsevier.com/locate/csite

Thermal degradation of KN90 gauze mask rope waste: Thermogravimetric and thermodynamic analyses, kinetic modeling and volatile products

Quanwei Li [a], Zhiyuan Zhao [b], Manjiang Yang [c], Ruiyu Chen [a,d,*]

[a] School of Chemistry and Chemical Engineering, Nanjing University of Science and Technology, Nanjing, Jiangsu, PR China
[b] Department of Infrastructure, Westlake University, Hangzhou, Zhejiang, PR China
[c] China Ship Development and Design Center, Wuhan, Hubei, PR China
[d] Department of Building Environment and Energy Engineering, The Hong Kong Polytechnic University, Kowloon, Hong Kong, PR China

ARTICLE INFO

Keywords:
KN90 gauze mask rope waste
Thermal degradation
Pyrolysis kinetics
Thermodynamic analysis
Volatile products

ABSTRACT

Pyrolysis is a promising thermal conversion method to dispose medical wastes. The pyrolysis behaviors, kinetics, thermodynamics and volatile products of KN90 gauze mask rope waste in nitrogen are studied under current study. The results indicate that two stages (stage 1: $0 \leq \alpha < 0.65$ and stage 2: $0.65 \leq \alpha \leq 1$) mainly constitute the pyrolysis process of KN90 gauze mask rope waste in nitrogen. The average values of activation energy for stage 1, stage 2 and the entire pyrolysis process are 254.79 kJ/mol, 340.96 kJ/mol and 285.21 kJ/mol, respectively. The thermal degradation in stage 2 can be regarded as one-step reaction. The average value of pre-exponential factor for stage 2 is 1.17×10^{24} min^{-1} $g(\alpha)=(1-\alpha)^{-2}-1$ can be adopted to characterize the thermal degradation in stage 2. The kinetic parameters for stage 2 can be adopted to well predict the conversion rate of stage 2. The variations of thermodynamic parameters suggest that the pyrolysis of KN90 gauze mask rope waste in nitrogen occurs more easily with the progress of thermal degradation. The total yield for the volatile products from most to least is alkanes > carbon dioxide > aromatic compounds > olefins > compounds containing carbonyl groups > alkynes > alcohols and water vapor. The possible chemical reactions to generate the specific volatile products are proposed.

1. Introduction

Wearing a gauze mask (N95 gauze mask, KN95 gauze mask, KN90 gauze mask, medical surgical mask, etc.) is an effective measure to prevent the spread of novel coronavirus and protect our health. Meanwhile, large quantities of mask wastes are produced. Owing to the potential novel coronavirus or other virus on the waste masks, it is inadvisable to dispose these waste gauze masks by landfill. Also, due to the potential pollution to the environment by releasing poisonous gases, incineration of these waste gauze masks cannot be considered as a good means. Pyrolysis, which is a kind of thermal conversion technologies and can effectively convert solid waste into useful chemical feedstocks and/or energy without environment contamination [1–3], may be a good alternative choice to handle such waste gauze masks.

The gauze mask mainly contains face mask and rope. The major constituent of the face mask is almost the same for various gauze

* Corresponding author. School of Chemistry and Chemical Engineering, Nanjing University of Science and Technology, Nanjing, Jiangsu, PR China.
E-mail address: crynjust@njust.edu.cn (R. Chen).

https://doi.org/10.1016/j.csite.2023.102816
Received 7 September 2022; Received in revised form 26 January 2023; Accepted 12 February 2023
Available online 14 February 2023

masks (polypropylene (PP)). However, the major constituent of the rope may be different for different gauze masks. For example, the major constituent of the rope for the KN90 gauze mask is polyisoprene, while the major constituents of the rope for the KN95 gauze mask and medical surgical mask are polyurethane (PU) and polyamide (PA) whose pyrolysis behaviors have received some attention [4,5]. The present study aims at the pyrolysis behaviors of the KN90 gauze mask rope with the major constituent of polyisoprene.

Some attention has been devoted to the pyrolysis of polyisoprene. First of all, the weight loss behaviors of polyisoprene in inert atmosphere (nitrogen or helium) was studied using thermogravimetric analysis under the single heating rate (10 K/min [6–8], 15 K/min [9], 40 K/min [10]) and multiple heating rates (2, 5 and 10 K/min [11], 5, 10, 15, 20, and 25 K/min [12], 10, 20 and 30 K/min [13]). Based on the thermogravimetric data and the assumption that the pyrolysis process of polyisoprene in inert atmosphere can be simply characterized by the reaction model $g(\alpha)=(1-\alpha)^n$ (α is conversion rate and n is order of reaction), the kinetic parameters including pre-exponential factor, activation energy and order of reaction were obtained. The obtained values of pre-exponential factor were 2.51×10^{20} min^{-1} [11], 7.92×10^{12} min^{-1} [12] and 3.92×10^{14} min^{-1} [13]. The obtained values of activation energy were 254 kJ/mol [11], 150 kJ/mol [12] and 187.76 kJ/mol [13]. The obtained values of order of reaction were 2.0 [11], 1.32 [12] and 1.72 [13]. It is indicated that large differences occur in the obtained values of kinetic parameters from different studies. Moreover, from the weight loss variations with temperature, the pyrolysis process of polyisoprene in inert atmosphere cannot be simply characterized by one reaction model. Thus, the accuracy of the obtained kinetic parameters values in the previous studies needs further validation. Besides, to date, thermodynamic analysis of the polyisoprene pyrolysis, which is based on the obtained kinetic parameters, has received little attention.

Besides the weight loss behaviors and kinetics, the pyrolytic products of polyisoprene in inert atmosphere were also reported in the previous studies. Jernejcic and Premru [14] employed gas chromatography (GC) to detect the pyrolytic products of polyisoprene in argon at the temperatures of 823, 873, 923, 973 and 1023 K. It was found that butane, isoprene, styrene, methyl styene and dipentene were the major pyrolytic products of polyisoprene in argon. In addition, isoprene, dipentene, diprene and 1,4- and 2,4-dimethyl-4-vinyl-cyclohexenes were detected in the pyrolytic products of polyisoprene in nitrogen at 773 K using GC by Galin [15]. However, Gelling et al. [16] reported that the major pyrolytic products of polyisoprene in nitrogen at 623 K were l-methyl-4-(1-methylethenyl) cyclohexene, l-methyl-4-(1-methylethy1) benzene and methyl-(1-methylethy1)cyclohexenes (an infrared spectroscopy and GC were used for the detection). And Cataldo [17] considered that dienes, trienes, tetraenes and aldehydic groups were the major pyrolytic products of polyisoprene in helium at the temperature range of 573–653 K. The pyrolytic products of polyisoprene in inert atmosphere were also studied at 863 K [18], 973 K [6], 553 K [11], 873 K [19], 973–1273 K [20], but the obtained results were different from each other. Furthermore, it is noted that previous studies mainly focused on the pyrolytic products of polyisoprene at fixed temperatures. The variations of the pyrolytic products of polyisoprene in the entire pyrolysis process still need to be addressed. Additionally, since polyisoprene is merely the major constituent of KN90 gauze mask rope, the pyrolysis behaviors of KN90 gauze mask rope may be different from those of polyisoprene. In summary, it is important and necessary to investigate the pyrolysis of KN90 gauze mask rope waste for chemical feedstocks and/or energy.

The present study aims at addressing the following issues: (1) the thermal decomposition behaviors of KN90 gauze mask rope waste in nitrogen at multiple heating rates; (2) the values for the kinetic parameters (pre-exponential factor, activation energy and reaction model); (3) accuracy of the obtained kinetic parameters values; (4) thermodynamic parameters values; (5) volatile products and potential chemical reactions.

2. Experimental setup and kinetic/thermodynamic theory

2.1. Experimental setup

As shown in Fig. 1, KN90 gauze mask rope waste was the studied material under current study. The KN90 gauze mask was manufactured by Minnesota Mining and Manufacturing (3 M) Corporation in Minnesota, USA. The major composition of KN90 gauze mask rope is polyisoprene. The rope was cut into small square pieces with each mass of approximately 4 mg for tests. The proximate and ultimate analyses results of KN90 gauze mask rope waste are listed in Table 1.

The thermal decomposition of KN90 gauze mask rope waste in nitrogen was characterized adopting a thermogravimetric analyzer with the product model of SDTA851E. The nitrogen flow rate was set to be 100 mL/min. The heating rates of 15, 20, 25 and 30 K/min

Fig. 1. KN90 gauze mask rope waste adopted under current study.

Table 1
Proximate and ultimate analyses results.

Proximate analysis (wt%)				Ultimate analysis (wt%)				
Moisture	Volatiles	ash	fixed carbon	C	H	N	O	S
1.6	96.56	0.12	1.72	87.47	11.16	0.87	0.49	0.01

and the temperature region of 450–850 K were selected for the thermogravimetric tests. Such heating rates and temperature region belong to those adopted in the slow/conventional pyrolysis reactors and are beneficial to the pyrolytic products generation in large proportion [21–25].

The volatile products generated by the decomposition of KN90 gauze mask rope waste in helium were monitored by a real-time TGA-FTIR-MS apparatus with the product model of TGA/DSC 3-Agilent 7890B–5977B-Nicolet iS50. The helium flow rate was also set to be 100 mL/min. The selected heating rate and temperature region were set be 20 K/min and 450–850 K, respectively. The basic theory for FTIR and MS to determine the volatile products is presented as follows. As to FTIR, different gases contain different function groups. The absorption peaks and intensity of the infrared radiation by different function groups are different. The types of volatile products are determined according to the absorption peaks and intensity in the FTIR spectra [26,27]. As to MS, the volatile products will be converted to fragment ions by electron ionization (EI). The generated fragment ions will be transported by electric or magnetic fields to the mass analyzer to generate mass spectra. Since different fragment ions possess different mass-to-charge ratio (m/z), the

Table 2
The common reaction model/mechanism of solid state pyrolysis [30,31].

No.	Symbol	$g(\alpha)$	$f(\alpha)$	Rate-determining mechanism
1. Chemical process or mechanism non-invoking equations				
1	$F_{1/3}$	$1-(1-\alpha)^{2/3}$	$3/2(1-\alpha)^{1/3}$	Chemical reaction
2	$F_{3/4}$	$1-(1-\alpha)^{1/4}$	$4(1-\alpha)^{3/4}$	Chemical reaction
3	$F_{3/2}$	$(1-\alpha)^{-1/2}-1$	$2(1-\alpha)^{3/2}$	Chemical reaction
4	F_2	$(1-\alpha)^{-1}-1$	$(1-\alpha)^2$	Chemical reaction
5	F_3	$(1-\alpha)^{-2}-1$	$1/2(1-\alpha)^3$	Chemical reaction
6	F_4	$(1-\alpha)^{-3}-1$	$1/3(1-\alpha)^4$	Chemical reaction
7	G_1	$1-(1-\alpha)^2$	$1/2(1-\alpha)$	Chemical reaction
8	G_2	$1-(1-\alpha)^3$	$1/3(1-\alpha)^2$	Chemical reaction
9	G_3	$1-(1-\alpha)^4$	$1/4(1-\alpha)^3$	Chemical reaction
2. Acceleratory rate equations				
10	$P_{3/2}$	$\alpha^{3/2}$	$2/3\alpha^{-1/2}$	Nucleation
11	$P_{1/2}$	$\alpha^{1/2}$	$2\alpha^{1/2}$	Nucleation
12	$P_{1/3}$	$\alpha^{1/3}$	$3\alpha^{2/3}$	Nucleation
13	$P_{1/4}$	$\alpha^{1/4}$	$4\alpha^{3/4}$	Nucleation
14	E_1	$ln\,\alpha$	α	Nucleation
3. Sigmoidal rate equations or random nucleation and subsequent growth				
15	A_1	$-ln(1-\alpha)$	$1-\alpha$	Assumed random nucleation and its subsequent growth
16	$A_{3/2}$	$[-ln(1-\alpha)]^{2/3}$	$3/2(1-\alpha)[-ln(1-\alpha)]^{1/3}$	Assumed random nucleation and its subsequent growth
17	A_2	$[-ln(1-\alpha)]^{1/2}$	$2(1-\alpha)[-ln(1-\alpha)]^{1/2}$	Assumed random nucleation and its subsequent growth
18	A_3	$[-ln(1-\alpha)]^{1/3}$	$3(1-\alpha)[-ln(1-\alpha)]^{2/3}$	Assumed random nucleation and its subsequent growth
19	A_4	$[-ln(1-\alpha)]^{1/4}$	$4(1-\alpha)[-ln(1-\alpha)]^{3/4}$	Assumed random nucleation and its subsequent growth
20	$A_{1/2}$	$[-ln(1-\alpha)]^2$	$1/2(1-\alpha)[-ln(1-\alpha)]^{-1}$	Assumed random nucleation and its subsequent growth
21	$A_{1/3}$	$[-ln(1-\alpha)]^3$	$1/3(1-\alpha)[-ln(1-\alpha)]^{-2}$	Assumed random nucleation and its subsequent growth
22	$A_{1/4}$	$[-ln(1-\alpha)]^4$	$1/4(1-\alpha)[-ln(1-\alpha)]^{-3}$	Assumed random nucleation and its subsequent growth
23	A_u	$ln\,\alpha/(1-\alpha)$	$\alpha/(1-\alpha)$	Branching nuclei
4. Deceleratory rate equations				
4.1. Phase boundary reaction				
24	R_1	α	1	Contracting disk
25	R_2	$1-(1-\alpha)^{1/2}$	$2(1-\alpha)^{1/2}$	Contracting cylinder (cylindrical symmetry)
26	R_3	$1-(1-\alpha)^{1/3}$	$3(1-\alpha)^{2/3}$	Contracting sphere (spherical symmetry)
4.2. Based on the diffusion mechanism				
27	D_1	$[1-(1-\alpha)^{1/2}]^{1/2}$	$4\{(1-\alpha)[1-(1-\alpha)]^{1/2}\}^{1/2}$	Two-dimensional diffusion
28	D_2	$\alpha+(1-\alpha)ln(1-\alpha)$	$[-ln(1-\alpha)]^{-1}$	Two-dimensional diffusion
29	D_3	$[1-(1-\alpha)^{1/3}]^2$	$(3/2)(1-\alpha)^{2/3}[1-(1-\alpha)^{1/3}]^{-1}$	Three-dimensional diffusion, spherical symmetry
30	D_4	$1-2/3\alpha-(1-\alpha)^{2/3}$	$(3/2)[(1-\alpha)^{-1/3}-1]^{-1}$	Three-dimensional diffusion, cylindrical symmetry
31	D_5	$[(1-\alpha)^{-1/3}-1]^2$	$(3/2)(1-\alpha)^{4/3}[(1-\alpha)^{-1/3}-1]^{-1}$	Three-dimensional diffusion
32	D_6	$[(1+\alpha)^{1/3}-1]^2$	$(3/2)(1+\alpha)^{2/3}[(1+\alpha)^{1/3}-1]^{-1}$	Three-dimensional diffusion
33	D_7	$1+2/3\alpha-(1+\alpha)^{2/3}$	$(3/2)[(1+\alpha)^{-1/3}-1]^{-1}$	Three-dimensional diffusion
34	D_8	$[(1+\alpha)^{-1/3}-1]^2$	$(3/2)(1+\alpha)^{4/3}[(1+\alpha)^{-1/3}-1]^{-1}$	Three-dimensional diffusion
35	D_9	$[1-(1-\alpha)^{1/3}]^{1/2}$	$6(1-\alpha)^{2/3}[1-(1-\alpha)^{1/3}]^{1/2}$	Three-dimensional diffusion

generated mass spectra based on the motion of different fragment ions from different volatile products are different. As a result, the types of volatile products can be determined by MS [26].

2.2. Kinetic theory

The solid pyrolysis behaviors can be described in the form of mathematical equations [28] shown as Equations (1) and (2) [29].

$$\frac{d\alpha}{dT}=\frac{A}{\beta}exp\left(-\frac{E}{RT}\right)f(\alpha) \tag{1}$$

$$g(\alpha)=\int_0^{\alpha}\frac{d\alpha}{f(\alpha)}=\frac{A}{\beta}\int_0^{T_\alpha}\exp\left(-\frac{E}{RT}\right)dT=-\frac{AE}{\beta R}\int_{y_\alpha}^{\infty}\frac{\exp(-y)}{y^2}dy=\frac{AE}{\beta R}p(y) \tag{2}$$

In equations (1) and (2), α, which is calculated by $\alpha=(m_0-m)/(m_0-m_\infty)$ (m_0 and m_∞ are the initial and final mass, respectively), denotes the conversion rate. T is the applied program temperature (K). A (min^{-1}), E (J/mol) and $f(\alpha)/g(\alpha)$ are the so-called kinetic triplet (pre-exponential factor, activation energy, reaction model (including its differential and integral form)). Note that the common reaction models and corresponding mechanism are presented in Table 2 β represents the temperature increase per minute (K/min). R is the universal gas constant (J/(mol·K)). y can be calculated by $y=E/(RT)$. y_α can be estimated by $y_\alpha=E/(RT_\alpha)$. It should be noted that there is no analytical solution for $p(y)$ ($p(y)=\int_{y_\alpha}^{\infty}\frac{exp(-y)}{y^2}dy$). For the purpose of kinetic calculation, many scholars put forward various approximate solutions for $p(y)$.

The kinetic methods used to calculate the kinetic parameters mainly contain model-free and model-fitting methods. In the current study, three popular model-free methods including KAS, FWO and Advanced Vyazovkin methods and one frequently-used model-fitting method i.e. CR method are adopted. As indicated in Table 3, for KAS and FWO methods, the E value at specific α can be obtained by the linear fitting of $\ln(\beta/T_\alpha^2)$ and $\ln\beta$ with $1/T_\alpha$ at the identical α under various heating rates, respectively. For the Advanced Vyazovkin method, the E value at specific α can be acquired by obtaining the minimum value of $\Omega(E_\alpha)$. For the CR method, it should be used based on the known or hypothetical $g(\alpha)$. In addition, the obtained E and A values are both the average values for one single-step decomposition process (note that the CR method is commonly applied for the single-step decomposition process, otherwise, inaccurate E and A values will be obtained). Specifically, the average E and A values are obtained by the linear fitting of $\ln(g(\alpha)/T^2)$ with $1/T$ at various temperatures for the single heating rate on the basis of one assumed $g(\alpha)$. If the estimated average E value by the CR method is close to that of model-free methods, then the corresponding $g(\alpha)$ can be considered to be capable of characterizing the single-step decomposition process.

2.3. Thermodynamic theory

Pyrolysis is a thermal and chemical conversion process. Thermodynamic parameters (the enthalpy change ΔH (J/mol)), Gibbs free energy change ΔG (J/mol), entropy change ΔS (J/(mol·K))) are commonly adopted to assess the favorability and difficulty for the occurrence of the solid thermal degradation. The specific calculation for ΔH, ΔG and ΔS are listed as follows.

$$A_\alpha=\beta E_\alpha e^{\left(E_\alpha/\left(RT_m^2\right)\right)}\Big/\left(RT_m^2\right) \tag{3}$$

$$\Delta H=E_\alpha-\mathrm{RT} \tag{4}$$

$$\Delta G=E_\alpha+\mathrm{RT}_m\,ln\left(\frac{k_BT_m}{hA_\alpha}\right) \tag{5}$$

$$\Delta S=\frac{\Delta H-\Delta G}{T_m} \tag{6}$$

In equations (3)–(6), T_m, k_B and h are the maximum temperature (K), Boltzmann constant (1.381×10^{-23} J/K) and Planck constant

Table 3
Typical approximation functions for $p(y)$ and corresponding kinetic methods.

Name	Approximation functions of $p(y)$	Specific functions
KAS method [32–34]	$p(y)=\frac{\exp(-y)}{y^2}$ [32]	$\ln(\beta/T_\alpha^2)=\ln(A_\alpha E_\alpha/Rg(\alpha))-E_\alpha/RT_\alpha$
FWO method [35–38]	$p(y)=\exp(-1.052y-5.331)$ [35]	$\ln\beta=\ln(A_\alpha E_\alpha/Rg(\alpha))-5.331-1.052(E_\alpha/RT_\alpha)$
Advanced Vyazovkin method [39–41]	$p(y)=\frac{exp(-y)}{y}\frac{y^5+40y^4+552y^3+3168y^2+7092y+4320}{y^6+42y^5+630y^4+4200y^3+12600y^2+15120y+5040}$ [42]	$\Omega(E_\alpha)=\sum_{i=1}^{n}\sum_{j\neq i}^{n}\frac{I(E_\alpha,T_{\alpha,i})\beta_j}{I(E_\alpha,T_{\alpha,j})\beta_i}$; $I(E_\alpha,T_\alpha)=\int_0^{T_\alpha}exp\left(-\frac{E_\alpha}{RT}\right)dT=\frac{E_\alpha}{R}p(y)$
CR method [43,44]	$p(y)=\frac{\exp(-y)}{y^2}\times\left(1+\frac{2!}{-y}\right)$ [32]	$\ln\frac{g(\alpha)}{T_\alpha^2}=\ln\left(\frac{A_\alpha R}{E_\alpha\beta}\right)-\frac{E_\alpha}{RT_\alpha}$

(6.626×10^{-34} J s), respectively.

3. Results and discussions

3.1. Thermogravimetric analysis

Fig. 2(a) and (b) illustrate α and $d\alpha/dT$ against temperature, respectively. Detailed information is listed in Table 4. It is indicated that the sample began to decompose at about 466–470 K and the decomposition ended at approximately 770–779 K. As depicted in Fig. 2(a), α increased slowly from 466 K to about 625 K and then increased rapidly in the temperature range of 625–760 K, afterwards, α increased slowly again. It is shown in Fig. 2(b) that $d\alpha/dT$ increased slowly from 466 K to about 600 K and then increased rapidly till 668 K, at which the first peak occurred. After the first peak temperature, $d\alpha/dT$ decreased rapidly from about 668 K to 700 K and then increased till about 720 K, at which the second peak occurred. Afterwards, $d\alpha/dT$ decreased sharply till 775 K and then remained almost zero till the end. It may be concluded that the decomposition process can be divided into two stages with the threshold of $\alpha = 0.65$ whose corresponding temperature is approximately 700 K. As indicated in Fig. 2 and Table 4, the first peak $d\alpha/dT$ increased with the heating rate β, which may be due to that the first peak temperature is relatively low, and the effect for the increase of T to increase $d\alpha/dT$ is larger than the effect for the increase of β to decrease $d\alpha/dT$. However, the second peak $d\alpha/dT$ decreased with β, which may be due to that the second peak temperature is relatively high, and the effect for the increase of T to increase $d\alpha/dT$ is lower than the effect for the increase of β to decrease $d\alpha/dT$.

3.2. Kinetic analysis

3.2.1. Kinetic analysis by model-free methods

As expounded in section 2.2, the activation energy E is closely related to the reaction rate $d\alpha/dT$ and will have a great influence on the thermal degradation behaviors. It is widely accepted that if E varies little in one certain degradation process, this degradation process may be nominally regarded as single-step reaction [45]. Fig. 3 and Table 5 present E as a function of α calculated by KAS, FWO and Advanced Vyazovkin methods. It is indicated that little difference occurs between the E values by the three methods at the identical α. E increased smoothly with α from $\alpha = 0.1$ to $\alpha = 0.65$. Afterwards, E remains almost stable. Based on the variations of E, the thermal degradation process can be divided into two stages with the threshold of $\alpha = 0.65$, which is consistent with that concluded by Fig. 2. Moreover, the thermal degradation in stage 2 can be nominally regarded as single-step reaction. The average E values for stage 1, stage 2 and the entire thermal degradation process are 254.79 kJ/mol, 340.96 kJ/mol and 285.21 kJ/mol, respectively.

3.2.2. Kinetic analysis by model-fitting method

It has now been proved that the thermal degradation in stage 2 can be nominally considered as single-step reaction. Thus, the model-fitting method (CR method is adopted in the current study) can be used to calculate the pre-exponential factor A and determine the reaction model $g(\alpha)$ for stage 2. On the basis of 36 reaction models, the corresponding E and $\ln A$ values were calculated by CR method and are presented in Table 6. Among the E values calculated based on the 36 reaction models, the E value calculated based on the No.5 reaction model $(1-\alpha)^{-2} - 1$ (313.73 kJ/mol) is closest to that calculated by the model-free methods (340.96 kJ/mol). Hence, $(1-\alpha)^{-2} - 1$ may be used to characterize the thermal degradation behaviors in stage 2. That is, chemical reaction is the main reaction mechanism in stage 2. It means that the reaction rate in stage 2 is directly proportional to the content, residual quantity or ratio of reactants raised to a particular power [46]. The A value for stage 2 can be calculated to be 1.17×10^{24} min^{-1} ($>6 \times 10^{10}$ min^{-1}), which indicates that a loose junctional complex is likely to occur in stage 2 [47].

The relationship between $\ln A$ and E is illustrated in Fig. 4. The values of relevant parameters including a, 95% confidence interval (CI) of a, b, 95% CI of b, k_{iso}, T_{iso} and correlation coefficient R^2 are listed in Table 7. It is shown that the T_{iso} value for all the heating rates is 650.51 K, which falls into the decomposition temperature range of the studied sample (466–779 K). It is widely reported that if the T_{iso} value falls into the decomposition temperature range, the reaction models selected for the kinetic calculation by the CR method

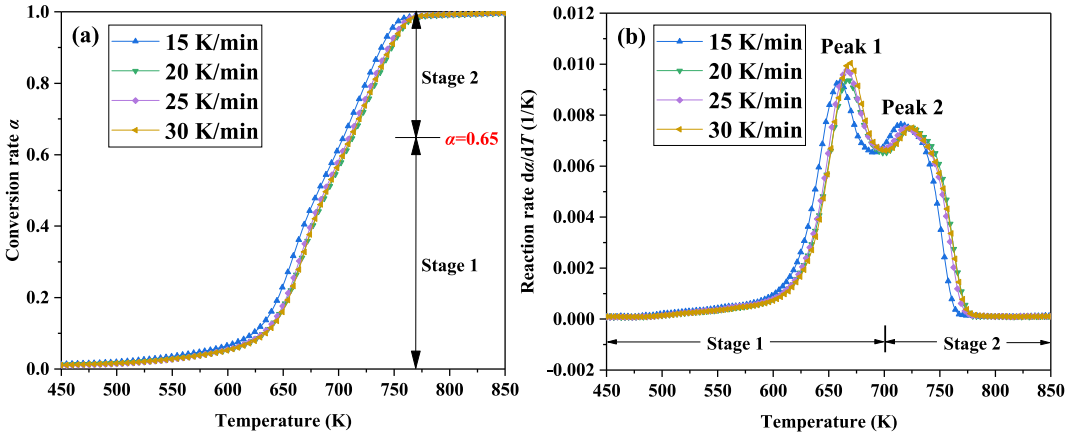

Fig. 2. α and $d\alpha/dT$ versus temperature.

Table 4
Thermogravimetric data.

β (K/min)	Peak 1			Peak 2			T_{onset} (K)	T_{end} (K)	Average dα/dT (1/K)
	dα/dT (1/K)	α	T (K)	dα/dT (1/K)	α	T (K)			
15	9.30×10^{-3}	0.33	660.40	7.64×10^{-3}	0.73	714.98	466.73	770.10	3.21×10^{-3}
20	9.37×10^{-3}	0.32	668.30	7.51×10^{-3}	0.74	725.23	467.16	780.33	3.11×10^{-3}
25	9.77×10^{-3}	0.32	666.13	7.50×10^{-3}	0.72	719.62	467.63	779.24	3.14×10^{-3}
30	1.00×10^{-2}	0.33	669.66	7.47×10^{-3}	0.73	722.56	469.09	778.38	3.16×10^{-3}

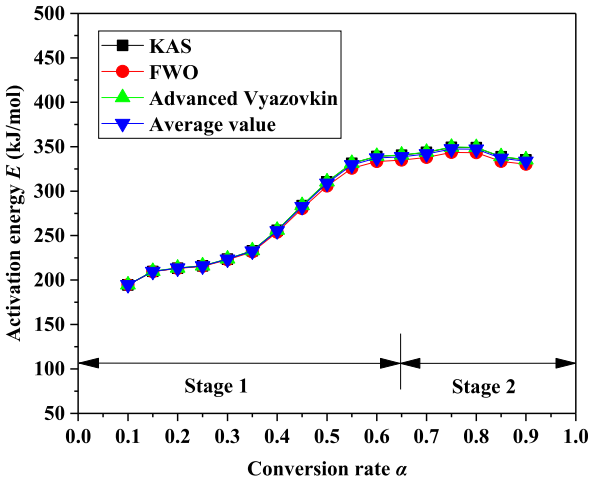

Fig. 3. E versus α through three model-free methods.

Table 5
E at different α through three model-free methods.

α	Activation energy E(kJ/mol)			
	KAS	FWO	Advanced Vyazovkin	Average value
0.10	194.44	194.65	194.70	194.60
0.15	209.73	209.40	209.99	209.70
0.20	213.35	212.96	213.61	213.31
0.25	215.78	215.37	216.04	215.73
0.30	223.55	222.84	223.81	223.40
0.35	232.82	231.74	233.07	232.54
0.40	255.88	253.75	256.11	255.25
0.45	283.68	280.29	283.90	282.62
0.50	310.31	305.73	310.52	308.86
0.55	331.26	325.76	331.45	329.49
0.60	339.10	333.34	339.30	337.25
0.65	340.51	334.80	340.71	338.67
0.70	343.64	337.88	343.84	341.79
0.75	349.42	343.48	349.62	347.51
0.80	349.04	343.22	349.24	347.17
0.85	338.66	333.46	338.88	337.00
0.90	335.19	330.27	335.41	333.62
Average value for the entire pyrolysis process	286.26	282.88	286.48	285.21
Average value for stage 1	255.45	253.26	255.68	254.79
Average value for stage 2	342.74	337.19	342.95	340.96

are appropriate [49]. Therefore, the 36 reaction models listed in Table 2 are considered as suitable for the kinetic calculation by the CR method.

3.2.3. *Validation and applicability of kinetic parameters*

Even though the kinetic triplet (E, A and $g(\alpha)$) for stage 2 have been obtained, their accuracy or applicability to predict the thermal degradation behaviors is still questioned since the adopted model-free and model-fitting methods are all proposed based on the approximate solutions of $p(y)$ and further simplified when they are finally applied in the kinetic calculation. Based on the approximate

Table 6
ln$A$, E and R^2 values through CR method.

No.	$g(\alpha)$	E (kJ/mol)	ln$A$ (min^{-1})	R^2
1	$1-(1-\alpha)^{1/3}$	44.05	4.99	0.99
2	$1-(1-\alpha)^{1/4}$	68.49	8.81	0.99
3	$(1-\alpha)^{-1/2}-1$	130.62	21.10	0.98
4	$(1-\alpha)^{-1}-1$	184.44	31.58	0.98
5	$(1-\alpha)^{-2}-1$	**313.73**	**55.42**	**0.96**
6	$(1-\alpha)^{-3}-1$	459.05	81.62	0.96
7	$1-(1-\alpha)^{2}$	3.24	−4.02	0.46
8	$1-(1-\alpha)^{3}$	−6.69	–	0.92
9	$1-(1-\alpha)^{4}$	−10.19	–	0.99
10	$\alpha^{3/2}$	49.79	6.14	0.99
11	$\alpha^{1/2}$	8.59	−2.22	0.98
12	$\alpha^{1/3}$	1.72	−4.93	0.79
13	$\alpha^{1/4}$	−1.71	–	0.87
14	$\ln\alpha$	0	–	–
15	$-\ln(1-\alpha)$	86.57	13.63	0.99
16	$[-\ln(1-\alpha)]^{2/3}$	53.71	7.54	0.99
17	$[-\ln(1-\alpha)]^{1/2}$	37.28	4.37	0.99
18	$[-\ln(1-\alpha)]^{1/3}$	20.85	0.98	0.99
19	$[-\ln(1-\alpha)]^{1/4}$	12.63	−0.92	0.98
20	$[-\ln(1-\alpha)]^{2}$	185.15	31.22	0.99
21	$[-\ln(1-\alpha)]^{3}$	283.73	48.49	0.99
22	$[-\ln(1-\alpha)]^{4}$	382.31	65.62	0.99
23	$\ln\alpha/(1-\alpha)$	0	–	–
24	α	29.19	2.31	0.99
25	$1-(1-\alpha)^{1/2}$	53.00	6.49	0.99
26	$1-(1-\alpha)^{1/3}$	63.04	8.04	0.99
27	α^{2}	70.39	9.79	0.99
28	$[1-(1-\alpha)^{1/2}]^{1/2}$	20.49	0.44	0.99
29	$\alpha+(1-\alpha)\ln(1-\alpha)$	97.08	14.25	0.99
30	$[1-(1-\alpha)^{1/3}]^{2}$	138.09	20.40	0.99
31	$1-2/3\alpha-(1-\alpha)^{2/3}$	110.34	15.23	0.99
32	$[(1-\alpha)^{-1/3}-1]^{2}$	241.59	39.24	0.99
33	$[(1+\alpha)^{1/3}-1]^{2}$	56.96	4.73	0.99
34	$1+2/3\alpha-(1+\alpha)^{2/3}$	61.18	5.64	0.99
35	$[(1+\alpha)^{-1/3}-1]^{2}$	45.04	2.13	0.99
36	$[1-(1-\alpha)^{1/3}]^{1/2}$	25.51	1.35	0.99

There is close relationship between the activation energy E and the pre-exponential factor A, which is called "kinetic compensation effects (KCE)" [48]. The specific function for KCE is $\ln A = a + bE$. Therein, a and b represent certain constants, and $a = \ln(k_{iso})$; $b = 1/(RT_{iso})$. k_{iso} denotes the nominal isokinetic rate constant. T_{iso} is the nominal isokinetic temperature.

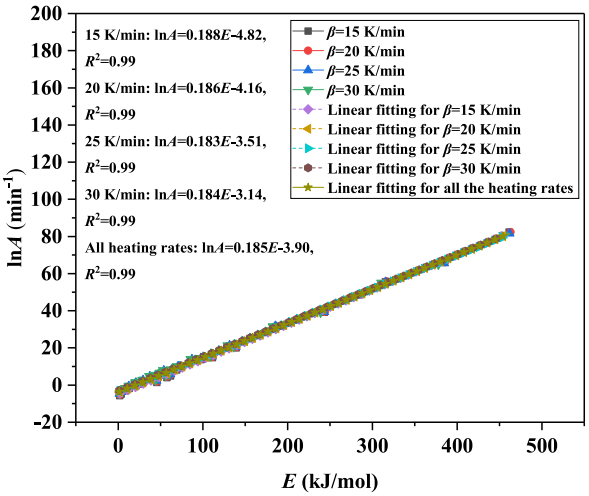

Fig. 4. Kinetic compensation effects (KCE) between ln$A$ and E.

Table 7
Relevant parameters for kinetic compensation effects.

β (K/min)	a (1/min)	CI for a	b (mol/kJ)	CI for b	k_{iso}	T_{iso} (K)	R^2
15	−4.82	(-5.39,-4.25)	1.88×10^{-1}	(0.18,0.19)	8.10×10^{-3}	641.28	0.99
20	−4.16	(-4.73,-3.58)	1.86×10^{-1}	(0.18,0.19)	1.57×10^{-2}	648.19	0.99
25	−3.51	(-4.09,-2.94)	1.83×10^{-1}	(0.18,0.19)	2.98×10^{-2}	657.33	0.99
30	−3.14	(-3.72,-2.56)	1.84×10^{-1}	(0.18,0.19)	4.34×10^{-2}	655.22	0.99
Total	−3.90	(-4.20,-3.60)	1.85×10^{-1}	(0.18,0.19)	2.02×10^{-2}	650.51	0.99

solutions of $p(y)$ for KAS method (as presented in Table 3) and the determined reaction model for stage 2 $g(\alpha) = (1-\alpha)^{-2} - 1$, α for stage 2 can be estimated using Equation (7).

$$\alpha = 1 - \sqrt{\frac{\beta R}{\beta R + AEp(y)}} \tag{7}$$

The predicted α versus temperature is compared with the experimental α against temperature for stage 2 at the heating rates of 15, 20, 25 and 30 K/min, as illustrated in Fig. 5. It is indicated that the predicted α agrees well with the experimental α for each heating rate. It may be concluded that the accuracy of the obtained E, A and $g(\alpha)$ for stage 2 is acceptable and can be applied to predict the thermal degradation behaviors of stage 2.

There are many types of polymer waste in the municipal waste. It is common to perform co-pyrolysis of different types of polymer waste for highly purified chemical feedstocks and fuels with high energy density. The decomposition temperature range and activation energy of different types of polymer waste have a great influence on the co-pyrolysis efficiency and pyrolytic products (purity, quantity, etc.). For example, polymer wastes with the same decomposition temperature range and activation energy are beneficial to effectively controlling the reactor temperatures. As shown in Table 8, the decomposition temperature range of KN90 gauze mask rope waste under current study is comparable with that of other polymer wastes. The average E value of KN90 gauze mask rope waste under current study is larger than that of all the listed polymer wastes except PS.

3.3. Thermodynamic analysis

Besides kinetic parameters, thermodynamic parameters including enthalpy change ΔH, Gibbs free energy change ΔG and entropy change ΔS also have a large effect on the thermal degradation process. The average values of ΔH, ΔG and ΔS and A for the calculation of ΔG in the cases of four heating rates (15, 20, 25 and 30 K/min) were calculated based on Eqs. (3)–(6) and presented in Fig. 6. It is shown in Fig. 6(b) and (d) that the ΔH and ΔS values both increased from $\alpha = 0.1$ to $\alpha = 0.65$ and then remained almost stable till the end, while the ΔG value decreased from $\alpha = 0.1$ to $\alpha = 0.65$ and then remained almost stable till the end, as illustrated in Fig. 6(c). From the variations of ΔH, ΔG and ΔS values with α, the thermal degradation process can be also divided into two stages with the threshold of $\alpha = 0.65$ and the thermal degradation in the second stage can be regarded as single-step reaction, which is consistent with that concluded by the reaction rate variations with temperature and activation energy variations with conversion rate. The average ΔH, ΔG and ΔS values for the whole thermal degradation process are 279.64 kJ/mol, 187.49 kJ/mol and 138.32 J/mol, respectively.

It is indicated in Fig. 6(b) that the ΔH values in the entire thermal degradation process are all positive, which suggests that the current thermal degradation process is endothermic [45]. Moreover, the increase in ΔH from $\alpha = 0.1$ to $\alpha = 0.65$ (stage 1) indicates that the thermal degradation in stage 1 requires more energy with the increase in α, while the little change of ΔH from $\alpha = 0.65$ to the

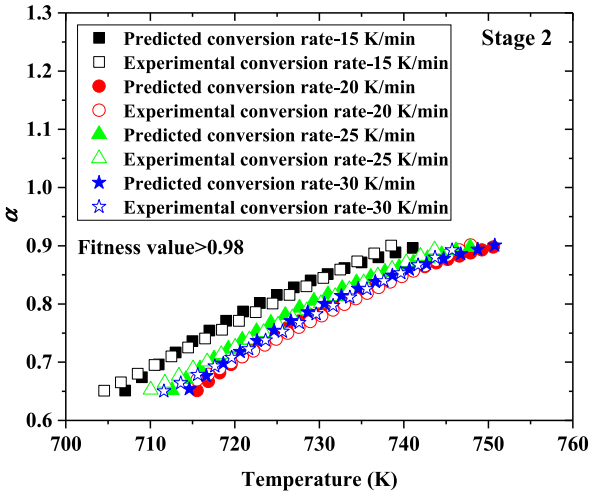

Fig. 5. Predicted α versus experimental α.

Table 8
Decomposition temperature range and E of typical polymers in inert atmosphere.

Specimen	Decomposition temperature range (K)	Average activation energy E (kJ/mol)	References
KN90 gauze mask rope waste (major composition: polyisoprene)	450–800	285.21	This study
Pure polyisoprene	523–748	150–254	[11–13]
Polyester FRP	373–803	63–164	[50,51]
Phenolic FRP	400–1056	217–239	[27]
Textile waste	378–873	38.18–169.3	[52–57]
PS	483–873	168–286	[49,58–62]
PMMA	423–793	116–269	[61,63–67]
LDPE	610–773	175–221	[58,59,68–70]
HDPE	523–783	238–264	[59,68,71–73]
PVC	473–873	72–242	[58,67,72, 74–76]
PET	473–793	117–260	[59,60,74,77]
PP	653–773	153–265	[58–60,68,72]
Tyres	300–773	33–283	[78–83]
Cellulose	520–700	148.46–240.23	[84–88]
PA	473–753	40–240	[4,89–91]
PU	400–1073	28.67–232.43	[5,49,62,92,93]

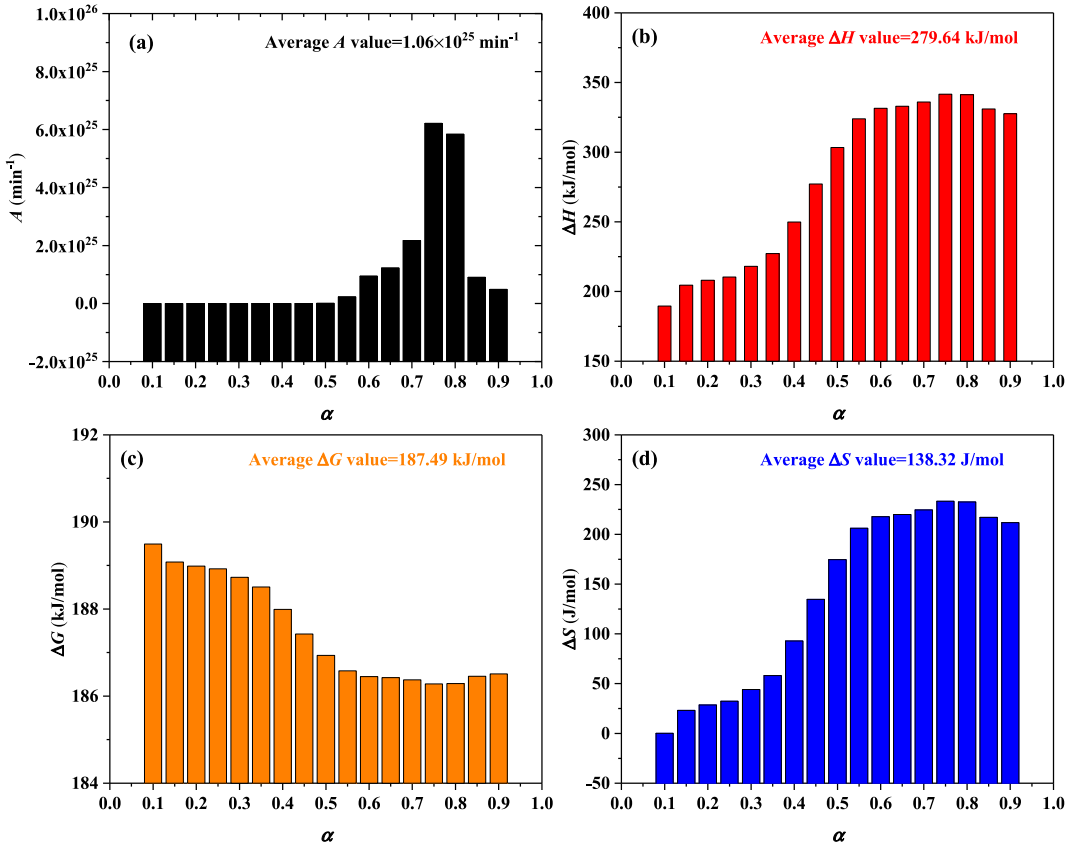

Fig. 6. Thermodynamic parameters versus α.

end (stage 2) suggests that the energy required for the thermal degradation in stage 2 remains almost stable. Note that the difference value between the average ΔH value and the average E value for the entire pyrolysis process is less than 7 kJ/mol, which is a low energy barrier and is beneficial for the generation of activated complex in the thermal degradation process [47].

ΔG denotes the feasibility for the occurrence of reactions [94]. The larger the ΔG value is, the lower the probability for the occurrence of reactions is. Hence, as shown in Fig. 6(c), the decrease in ΔG from $\alpha = 0.1$ to $\alpha = 0.65$ (stage 1) suggests that the thermal degradation in stage 1 occurs more easily with the increase in α. The little change in ΔG from $\alpha = 0.65$ to the end (stage 2) indicates that

the probability for the occurrence of thermal degradation in stage 2 remains nearly stable. Furthermore, the ΔG values in the whole thermal degradation process are all positive, which indicates that the thermal degradation in the current study is non-spontaneous [45].

ΔS is highly related to the reaction disorder degree in the thermal degradation process [94]. Large ΔS value represents that the reactivity for the thermal degradation is high and it is difficult for the reaction system to reach the thermodynamic equilibrium. As depicted in Fig. 6(d), the increase in ΔS from $\alpha = 0.1$ to $\alpha = 0.65$ (stage 1) indicates that the reaction disorder degree becomes larger with the increase in α in stage 1. The little change in ΔS from $\alpha = 0.65$ to the end (stage 2) suggests that the reaction disorder degree remains almost constant in stage 2.

3.4. Volatile product analysis

Recycling valuable chemical feedstocks and fuels from the volatile products of polymer waste pyrolysis is one of the goals for solid waste pyrolysis. Thus, it is important to analyze the volatile products occurring in the solid waste pyrolysis process. Even though the gases used for the thermogravimetric tests (nitrogen) and online TGA-FTIR-MS tests (helium) are different, the α and $d\alpha/dT$ variations with temperature under nitrogen and helium are almost the same. Hence, the α and $d\alpha/dT$ variations with temperature under helium are not illustrated here to avoid repetition.

The infrared spectra for volatile gases at peaks 1 and 2 are illustrated in Fig. 7. The functional groups corresponding to the absorption peaks are further presented in Table 9. It is indicated that olefins, alcohols and/or water vapor, alkanes, compounds containing carbonyl groups, alkynes, aromatic compounds and carbon dioxide mainly occur in the volatile products.

The variations of seven types of volatile products as a function of time are depicted in Fig. 8(a). As to the absorbance for alkanes, olefins, compounds containing carbonyl groups, alkynes and aromatic compounds, it increased smoothly from approximately 15 min–21 min and attained peak 1 at 21 min. And then a decrease occurred. As to the absorbance for carbon dioxide and alcohols and/or water vapor, it began to increase at about 22.5 min and reached peak 2 at about 30 min. The maximum absorbance of volatile products from most to least is carbon dioxide > alkanes > aromatic compounds > olefins > alcohols and/or water vapor > compounds containing carbonyl groups > alkynes, as shown in Fig. 8(b). The total yield (percentage) for the seven types of volatile products are illustrated in Fig. 9, which suggests that the total yield for volatile products from most to least is alkanes (36.42%)>carbon dioxide

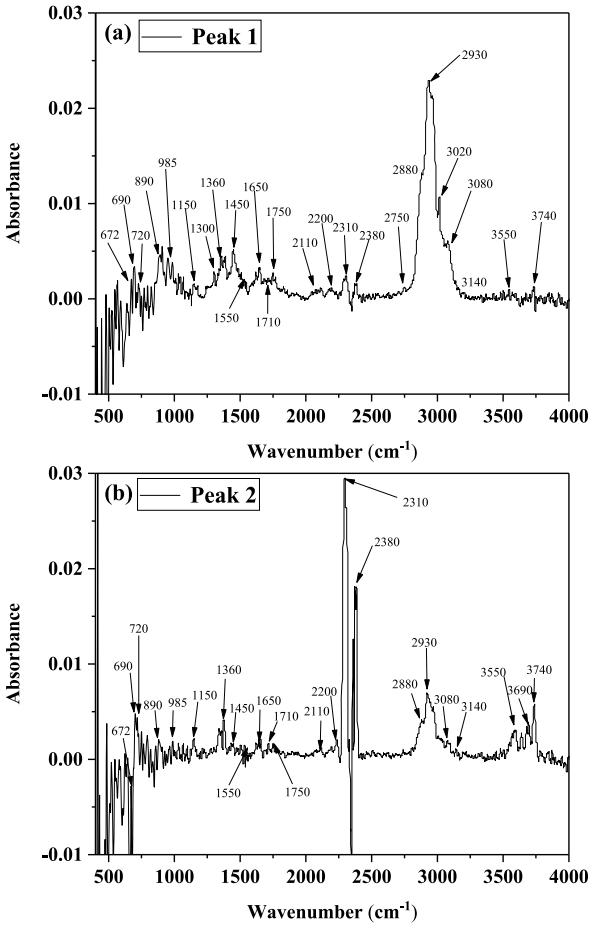

Fig. 7. Infrared spectra for volatile gases at peaks 1 and 2.

Table 9
Functional groups concluded by the absorption bands in the infrared spectra [95,96].

Number	Typical peaks (1/cm)	Function groups	Vibration	Products
1	690, 890, 985,	C–H in olefins	Deformation	Olefins
	3080		Stretching	
	1650	C=C in olefins	Stretching	
2	1150	C–O in alcohols	Stretching	Alcohols and/or water vapor
	1300	O–H	Deformation	
	3140, 3550, 3690, 3740		Stretching	
3	1360, 2880, 2930	C–H in alkanes	Stretching	Alkanes
	1450, 1640		Deformation	
4	1710, 1750	C=O in compounds containing carbonyl groups	Stretching	Compounds containing carbonyl groups
	2750	C–H in compounds containing carbonyl groups		
5	2110, 2200	C≡C in alkynes	Stretching	Alkynes
6	3020	C–H in aromatic compounds	Stretching	Aromatic compounds
	1550	C=C in aromatic compounds	Skeleton vibration	
	720	C–H in aromatic compounds	Out-of-plane bending	
7	2310, 2380	C=O in carbon dioxide	Stretching	Carbon dioxide
	672		Deformation	

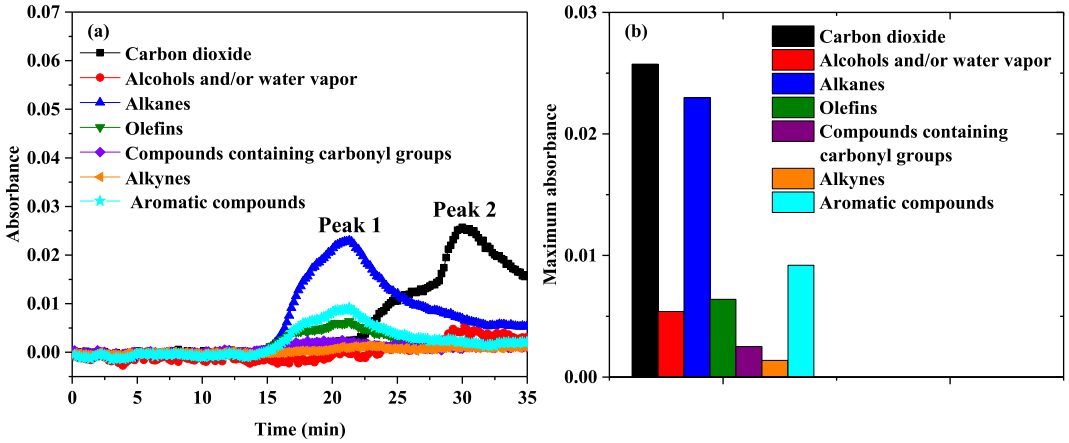

Fig. 8. (a) Absorbance of volatile products; (b) Maximum absorbance of volatile products.

(35.45%)>aromatic compounds (11.63%)>olefins (9.94%)>compounds containing carbonyl groups (4.2%)>alkynes (1.87%)>alcohols and/or water vapor (0.49%).

The major functional groups of the volatile products have been now identified by FTIR. The specific volatile products are further determined by MS on the basis of FTIR results, as listed in Table 10. It is shown that carbon dioxide, alcohols (methyl alcohol), water

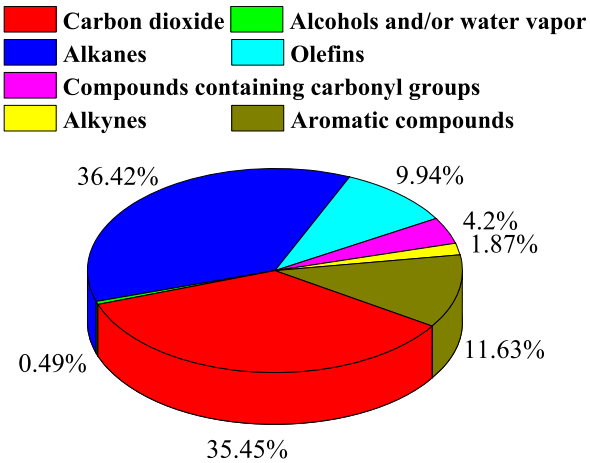

Fig. 9. Total yield (percentage) of volatile products.

vapor, alkanes (methane, ethane, butane, pentane, 2-methylpentane, 4-methylheptane), olefins (ethylene, 1,3-butadiene, 2-butylene, 2-methyl-1-pentene, 4-methyl-2-pentene, 2,3-dimethyl-1,3-pentadiene, nonadeca-1,3,5-triene), aldehydes (formaldehyde, acetaldehyde), ketones (acetone, butanone), carboxylic acids (formic acid, acetic acid), esters (δ-Hexanolactone), alkynes (acetylene, 2,4-hexadiyne) and aromatic compounds (benzene, methylbenzene) occurred in the volatile products. The generation of olefins may be due to the breakage of branched chain or chain backbone. By capturing the free radicals (hydrogen ion, methyl, methylene, etc.), the generated olefins can be transformed into alkanes. If the free radicals (hydrogen ion, methyl, methylene, etc.) are broken away from the generated olefins, alkynes will be formed. Through the oxidation of the free methyl and methylene by the free hydroxide radical generated from the decomposition of water vapor, the methyl alcohol may be formed. The carbon-carbon double bond is quite active, it can be oxidized by the free hydroxide radical. Then aldehydes, ketones and esters are generated. Through the further oxidation of the generated aldehydes, ketones and esters by the free hydroxide radical, carboxylic acids may be formed. Carbon dioxide may be generated due to the dehydrogenation of the formed carboxyl. As to the aromatic compounds, they may be formed by the cycloaddition of olefins.

4. Conclusions

(1) Two peaks occur in the reaction rate curves of the KN90 gauze mask rope waste in nitrogen. The first peak reaction rate increases with the heating rate, while the second peak reaction rate decreases with the heating rate. Two stages (stage 1: $0 \leq \alpha < 0.65$ and stage 2: $0.65 \leq \alpha \leq 1$) mainly constitute the pyrolysis process of the KN90 gauze mask rope waste with the major composition of polyisoprene in nitrogen.

(2) The average values of activation energy for stage 1, stage 2 and the entire pyrolysis process are 254.79 kJ/mol, 340.96 kJ/mol and 285.21 kJ/mol, respectively. The thermal degradation in stage 2 can be regarded as one-step reaction. The average value of pre-exponential factor for stage 2 is 1.17×10^{24} min^{-1}. $g(\alpha) = (1-\alpha)^{-2} - 1$ can be adopted to characterize the thermal degradation in stage 2. These three obtained kinetic parameters for stage 2 can be adopted to well predict the conversion rate of stage 2. In addition, the decomposition temperature range of the KN90 gauze mask rope waste under current study is comparable with that of other common polymer wastes. The average activation energy value for the entire pyrolysis process of the KN90 gauze mask rope waste under current study is larger than that of most common polymer wastes.

(3) The ΔH and ΔS values increase with the conversion rate in stage 1 and remain almost constant in stage 2, while the ΔG value decreases with the conversion rate in stage 1 and remains nearly constant in stage 2. The variations of ΔH, ΔG and ΔS values suggest that the pyrolysis of the KN90 gauze mask rope waste in nitrogen occurs more easily with the progress of thermal degradation. Additionally, the average ΔH, ΔG and ΔS values for the whole thermal degradation process are 279.64 kJ/mol, 187.49 kJ/mol and 138.32 J/mol, respectively.

(4) Carbon dioxide, alcohols (methyl alcohol), water vapor, alkanes (methane, ethane, butane, pentane, 2-methylpentane, 4-methylheptane), olefins (ethylene, 1,3-butadiene, 2-butylene, 2-methyl-1-pentene, 4-methyl-2-pentene, 2,3-dimethyl-1,3-pentadiene, nonadeca-1,3,5-triene), aldehydes (formaldehyde, acetaldehyde), ketones (acetone, butanone), carboxylic acids

Table 10
Possible pyrolytic gases determined through MS.

No.	Possible products	Formula	molecular weight	Family
1	carbon dioxide	CO_2	44	inorganic substances
2	methyl alcohol	CH_4O	32	alcohols
3	water	H_2O	18	inorganic substances
4	methane	CH_4	16	alkanes
	ethane	C_2H_6	30	
	butane	C_4H_{10}	58	
	pentane	C_5H_{12}	72	
	2-methylpentane	C_6H_{14}	86	
	4-methylheptane	C_8H_{18}	114	
5	ethylene	C_2H_4	28	olefins
	1,3-butadiene	C_4H_6	54	
	2-butylene	C_4H_8	56	
	2-methyl-1-pentene	C_6H_{12}	84	
	4-methyl-2-pentene	C_6H_{12}	84	
	2,3-dimethyl-1,3-pentadiene	C_7H_{12}	96	
	nonadeca-1,3,5-triene	$C_{19}H_{34}$	262	
6	formaldehyde	HCHO	30	aldehydes
	acetaldehyde	C_2H_4O	44	
7	acetone	C_3H_6O	58	ketones
	butanone	C_4H_8O	72	
8	formic acid	HCOOH	46	carboxylic acids
	acetic acid	$C_2H_4O_2$	60	
9	δ-Hexanolactone	$C_6H_{10}O_2$	114	esters
10	acetylene	C_2H_2	26	alkynes
	2,4-hexadiyne	C_6H_6	78	
11	benzene	C_6H_6	78	aromatic compounds
	methylbenzene	C_7H_8	92	

(formic acid, acetic acid), esters (δ-Hexanolactone), alkynes (acetylene, 2,4-hexadiyne) and aromatic compounds (benzene, methylbenzene) occur in the volatile products. The possible chemical reactions to generate the above-mentioned products are proposed. The total yield for the volatile products from most to least is alkanes > carbon dioxide > aromatic compounds > olefins > compounds containing carbonyl groups (aldehydes, ketones, carboxylic acids, esters)>alkynes > alcohols and water vapor.

Author statement

Quanwei Li: Methodology, Investigation, Formal analysis, Validation, Writing-Original Draft, Zhiyuan Zhao: Methodology, Formal analysis, Data Curation, Writing-review & editing, Manjiang Yang: Validation, Resources, Investigation, Ruiyu Chen: Conceptualization, Methodology, Supervision, Project administration.

Declaration of competing interest

The authors declare that they have no known competing financial interests or personal relationships that could have appeared to influence the work reported in this paper.

Data availability

Data will be made available on request.

Acknowledgments

This work was sponsored by Hong Kong Scholars Program (No. XJ2021025), National Natural Science Foundation of China (No. 52276119), China Postdoctoral Science Foundation (No. 2020M680069) and Jiangsu Planned Projects for Postdoctoral Research Funds (No. 2020Z414).

References

[1] M. Ashraf, N. Ramzan, R.U. Khan, A.K. Durrani, Analysis of mixed cattle manure: kinetics and thermodynamic comparison of pyrolysis and combustion processes, Case Stud. Therm. Eng. 26 (2021), 101078.
[2] P. Mankeed, T. Onsree, S.R. Naqvi, S. Shimpalee, N. Tippayawong, Kinetic and thermodynamic analyses for pyrolysis of hemp hurds using discrete distributed activation energy model, Case Stud. Therm. Eng. 31 (2022), 101870.
[3] Z. Wang, S. Hostikka, J. Wang, Pyrolysis behavior and kinetic analysis of waste polypropylene-based complex for cable filler, Case Stud. Therm. Eng. 37 (2022), 102261.
[4] S.V. Levchik, E.D. Weil, M. Lewin, Thermal decomposition of aliphatic nylons, Polym. Int. 48 (1999) 532–557.
[5] K. Li, D.S. Pau, H. Zhang, Pyrolysis of polyurethane foam: optimized search for kinetic properties via simultaneous K–K method, genetic algorithm and elemental analysis, Fire Mater. 40 (2016) 800–817.
[6] G. San Miguel, J. Aguado, D. Serrano, J. Escola, Thermal and catalytic conversion of used tyre rubber and its polymeric constituents using Py-GC/MS, Appl. Catal. B Environ. 64 (2006) 209–219.
[7] T. Kan, V. Strezov, T. Evans, Fuel production from pyrolysis of natural and synthetic rubbers, Fuel 191 (2017) 403–410.
[8] P. Song, X. Wu, S. Wang, Effect of styrene butadiene rubber on the light pyrolysis of the natural rubber, Polym. Degrad. Stabil. 147 (2018) 168–176.
[9] X. Wei, H. Zhong, Q. Yang, E. Yao, Y. Zhang, H. Zou, Studying the mechanisms of natural rubber pyrolysis gas generation using RMD simulations and TG-FTIR experiments, Energy Convers. Manag. 189 (2019) 143–152.
[10] M.J. Fernández-Berridi, N. González, A. Mugica, C. Bernicot, Pyrolysis-FTIR and TGA techniques as tools in the characterization of blends of natural rubber and SBR, Thermochim. Acta 444 (2006) 65–70.
[11] S. Seidelt, M. Müller-Hagedorn, H. Bockhorn, Description of tire pyrolysis by thermal degradation behaviour of main components, J. Anal. Appl. Pyrol. 75 (2006) 11–18.
[12] B. Lah, D. Klinar, B. Likozar, Pyrolysis of natural, butadiene, styrene–butadiene rubber and tyre components: modelling kinetics and transport phenomena at different heating rates and formulations, Chem. Eng. Sci. 87 (2013) 1–13.
[13] S. Liu, J. Yu, K. Bikane, T. Chen, C. Ma, B. Wang, et al., Rubber pyrolysis: kinetic modeling and vulcanization effects, Energy 155 (2018) 215–225.
[14] M. Jernejcic, L. Premru, Pyrolysis gas chromatography of natural rubber and synthetic polyisoprene, Rubber Chem. Technol. 41 (1968) 411–417.
[15] M. Galin, Study of polyisoprene microstructure by flash pyrolysis gas chromatography, J. Macromol. Sci.-Chem. 7 (1973) 873–888.
[16] I. Gelling, M. Loadman, B. Sidek, Pyrolysis of polyisoprenes. I. Differentiation between natural and synthetic cis-1, 4-polyisoprenes, J. Polym. Sci. Polym. Chem. Ed. 17 (1979) 1383–1392.
[17] F. Cataldo, Thermal depolymerization and pyrolysis of cis-1, 4-polyisoprene: preparation of liquid polyisoprene and terpene resin, J. Anal. Appl. Pyrol. 44 (1998) 121–130.
[18] S.S. Choi, Correlation of crosslink density with pyrolysis pattern of natural rubber vulcanizates with efficient vulcanizing cure system, J. Anal. Appl. Pyrol. 52 (1999) 105–112.
[19] W. Kaminsky, C. Mennerich, Z. Zhang, Feedstock recycling of synthetic and natural rubber by pyrolysis in a fluidized bed, J. Anal. Appl. Pyrol. 85 (2009) 334–337.
[20] F. Xu, B. Wang, D. Yang, X. Ming, Y. Jiang, J. Hao, et al., TG-FTIR and Py-GC/MS study on pyrolysis mechanism and products distribution of waste bicycle tire, Energy Convers. Manag. 175 (2018) 288–297.
[21] A. Demirbas, Determination of calorific values of bio-chars and pyro-oils from pyrolysis of beech trunkbarks, J. Anal. Appl. Pyrol. 72 (2004) 215–219.
[22] A.H. Demirbaåž, Yields and heating values of liquids and chars from spruce trunkbark pyrolysis, Energy Sources 27 (2005) 1367–1373.
[23] N. Tippayawong, J. Kinorn, S. Thavornun, Yields and gaseous composition from slow pyrolysis of refuse-derived fuels, Energy Sources 30 (2008) 1572–1580.
[24] R. Chen, Q. Li, X. Xu, D. Zhang, Pyrolysis kinetics and reaction mechanism of representative non-charring polymer waste with micron particle size, Energy Convers. Manag. 198 (2019), 111923.
[25] J. Huang, J. Liu, J. Chen, W. Xie, J. Kuo, X. Lu, et al., Combustion behaviors of spent mushroom substrate using TG-MS and TG-FTIR: thermal conversion, kinetic, thermodynamic and emission analyses, Bioresour. Technol. 266 (2018) 389–397.
[26] R. Chen, S. Lu, Y. Zhang, S. Lo, Pyrolysis study of waste cable hose with thermogravimetry/Fourier transform infrared/mass spectrometry analysis, Energy Convers. Manag. 153 (2017) 83–92.

[27] R. Chen, X. Xu, S. Lu, Y. Zhang, S. Lo, Pyrolysis study of waste phenolic fibre-reinforced plastic by thermogravimetry/Fourier transform infrared/mass spectrometry analysis, Energy Convers. Manag. 165 (2018) 555–566.
[28] T. Onsree, N. Tippayawong, A. Zheng, H. Li, Pyrolysis behavior and kinetics of corn residue pellets and eucalyptus wood chips in a macro thermogravimetric analyzer, Case Stud. Therm. Eng. 12 (2018) 546–556.
[29] W. Xu, J. Liu, Z. Ding, J. Fu, F. Evrendilek, W. Xie, et al., Dynamic pyrolytic reaction mechanisms, pathways, and products of medical masks and infusion tubes, Sci. Total Environ. 842 (2022), 156710.
[30] L. Liqing, C. Donghua, Application of iso-temperature method of multiple rate to kinetic analysis, J. Therm. Anal. Calorim. 78 (2004) 283–293.
[31] Z. Ding, H. Chen, J. Liu, H. Cai, F. Evrendilek, M. Buyukada, Pyrolysis dynamics of two medical plastic wastes: drivers, behaviors, evolved gases, reaction mechanisms, and pathways, J. Hazard Mater. 402 (2021), 123472.
[32] P. Murray, J. White, Kinetics of the thermal dehydration of clays. Part IV. Interpretation of the differential thermal analysis of the clay minerals, Trans. J. Br. Ceram. Soc. 54 (1955) 204–238.
[33] H.E. Kissinger, Variation of peak temperature with heating rate in differential thermal analysis, J. Res. Natl. Bur. Stand. 57 (1956) 217–221.
[34] T. Akahira, T. Sunose, Research Report, Joint Convention of Four Electrical Institutes, vol. 16, Chiba Institute of Technology, 1971, pp. 22–31.
[35] C.D. Doyle, Estimating isothermal life from thermogravimetric data, J. Appl. Polym. Sci. 6 (1962) 639–642.
[36] T. Ozawa, A new method of analyzing thermogravimetric data, Bull. Chem. Soc. Jpn. 38 (1965) 1881–1886.
[37] J.H. Flynn, L.A. Wall, A. quick, Direct method for the determination of activation energy from thermogravimetric data, J. Polym. Sci. C Polym. Lett. 4 (1966) 323–328.
[38] J. Flynn, The isoconversional method for determination of energy of activation at constant heating rates, J. Therm. Anal. Calorim. 27 (1983) 95–102.
[39] S. Vyazovkin, D. Dollimore, Linear and nonlinear procedures in isoconversional computations of the activation energy of nonisothermal reactions in solids, J. Chem. Inf. Model. 36 (1996) 42–45.
[40] S. Vyazovkin, Advanced isoconversional method, J. Therm. Anal. 49 (1997) 1493–1499.
[41] S. Vyazovkin, Evaluation of activation energy of thermally stimulated solid-state reactions under arbitrary variation of temperature, J. Comput. Chem. 18 (2015) 393–402.
[42] J. Farjas, P. Roura, Isoconversional analysis of solid state transformations, J. Therm. Anal. Calorim. 105 (2011) 757–766.
[43] A.W. Coats, J. Redfern, Kinetic parameters from thermogravimetric data, Nature 201 (1964) 68–69.
[44] A. Coats, J. Redfern, Kinetic parameters from thermogravimetric data. II, J. Polym. Sci. C Polym. Lett. 3 (1965) 917–920.
[45] R. Chen, D. Zhang, X. Xu, YougenYuan. Pyrolysis characteristics, kinetics, thermodynamics and volatile products of waste medical surgical mask rope by thermogravimetry and online thermogravimetry-Fourier transform infrared-mass spectrometry analysis, Fuel 295 (2021), 120632.
[46] A. Khawam, D.R. Flanagan, Solid-state kinetic models: basics and mathematical fundamentals, ChemInform 110 (2006) 17315–17328.
[47] M. Barbanera, F. Cotana, U. Di Matteo, Co-combustion performance and kinetic study of solid digestate with gasification biochar, Renew. Energy 121 (2018) 597–605.
[48] S. Vyazovkin, A.K. Burnham, J.M. Criado, L.A. Pérez-Maqueda, C. Popescu, N. Sbirrazzuoli, ICTAC Kinetics Committee recommendations for performing kinetic computations on thermal analysis data, Thermochim. Acta 520 (2011) 1–19.
[49] L. Jiang, D. Zhang, M. Li, J.J. He, Z.H. Gao, Y. Zhou, et al., Pyrolytic behavior of waste extruded polystyrene and rigid polyurethane by multi kinetics methods and Py-GC/MS, Fuel 222 (2018) 11–20.
[50] Y.M. Yun, M.W. Seo, G.H. Koo, H.W. Ra, S.J. Yoon, Y.K. Kim, et al., Pyrolysis characteristics of GFRP (glass fiber reinforced plastic) under non-isothermal conditions, Fuel 137 (2014) 321–327.
[51] B. Yu, V. Till, K. Thomas, Modeling of thermo-physical properties for FRP composites under elevated and high temperature, Compos. Sci. Technol. 67 (2007) 3098–3109.
[52] R. Miranda, C. Sosa_Blanco, D. Bustos-Martínez, C. Vasile, Pyrolysis of textile wastes: I. Kinetics and yields, J. Anal. Appl. Pyrol. 80 (2007) 489–495.
[53] R. Chowdhury, A. Sarkar, Reaction kinetics and product distribution of slow pyrolysis of Indian textile wastes, Int. J. Chem. React. Eng. 10 (2012) 1–23.
[54] R. Chowdhury, S. Poddar, S. De, Kinetic modelling of non-catalytic pyrolysis of waste jute in a fixed bed pyrolyzer, APCBEE Procedia 9 (2014) 18–24.
[55] F. Zhu, Q. Feng, Y. Xu, R. Liu, K. Li, Kinetics of pyrolysis of ramie fabric wastes from thermogravimetric data, J. Therm. Anal. Calorim. 119 (2015) 651–657.
[56] C. Wen, Y. Wu, X. Chen, G. Jiang, D. Liu, The pyrolysis and gasification performances of waste textile under carbon dioxide atmosphere, J. Therm. Anal. Calorim. 128 (2016) 581–591.
[57] M. Zhang, Q. Yuan, D. Huang, Y. Hu, S. Wang, L. Shen, Study of thermal stability and thermodynamics of typical textiles, China Sciencepaper 13 (2018) 2117–2123.
[58] S.P. Sang, K.S. Dong, H.L. Sang, T.U. Yu, J. Hwang, Study on pyrolysis characteristics of refuse plastic fuel using lab-scale tube furnace and thermogravimetric analysis reactor, J. Anal. Appl. Pyrol. 97 (2012) 29–38.
[59] S.D.A. Sharuddin, F. Abnisa, M.A.W.D. Wan, M.K. Aroua, Energy recovery from pyrolysis of plastic waste: study on non-recycled plastics (NRP) data as the real measure of plastic waste, Energy Convers. Manag. 148 (2017) 925–934.
[60] J.M. Encinar, J.F. González, Pyrolysis of synthetic polymers and plastic wastes. Kinetic study, Fuel Process. Technol. 89 (2008) 678–686.
[61] H.R. Azimi, M. Rezaei, F. Majidi, The non-isothermal degradation kinetics of St-MMA copolymers, Polym. Degrad. Stabil. 99 (2014) 240–248.
[62] L. Jiang, H. Xiao, J. He, Q. Sun, L. Gong, J. Sun, Application of genetic algorithm to pyrolysis of typical polymers, Fuel Process. Technol. 138 (2015) 48–55.
[63] B.S. Kang, G.K. Sang, J.S. Kim, Thermal degradation of poly(methyl methacrylate) polymers: kinetics and recovery of monomers using a fluidized bed reactor, J. Anal. Appl. Pyrol. 81 (2008) 7–13.
[64] G. Lopez, M. Artetxe, M. Amutio, G. Elordi, R. Aguado, M. Olazar, et al., Recycling poly-(methyl methacrylate) by pyrolysis in a conical spouted bed reactor, Chem. Eng. Process: Process Intensif. 49 (2010) 1089–1094.
[65] M. Ferriol, A. Gentilhomme, M. Cochez, N. Oget, J.L. Mieloszynski, Thermal degradation of poly(methyl methacrylate) (PMMA): modelling of DTG and TG curves, Polym. Degrad. Stabil. 79 (2003) 271–281.
[66] J. Cheng, Y. Pan, J. Yao, X. Wang, F. Pan, J. Jiang, Mechanisms and kinetics studies on the thermal decomposition of micron Poly(methyl methacrylate) and polystyrene, J. Loss Prev. Process. Ind. 40 (2016) 139–146.
[67] A. Bhargava, P.V. Hees, B. Andersson, Pyrolysis modeling of PVC and PMMA using a distributed reactivity model, Polym. Degrad. Stabil. 129 (2016) 199–211.
[68] A. Aboulkas, K.E. Harfi, A.E. Bouadili, Thermal degradation behaviors of polyethylene and polypropylene. Part I: pyrolysis kinetics and mechanisms, Energy Convers. Manag. 51 (2010) 1363–1369.
[69] B. Saha, A.K. Ghoshal, Model-free kinetics analysis of ZSM-5 catalyzed pyrolysis of waste LDPE, Thermochim. Acta 453 (2007) 120–127.
[70] S. Sharma, A.K. Ghoshal, Study of kinetics of co-pyrolysis of coal and waste LDPE blends under argon atmosphere, Fuel 89 (2010) 3943–3951.
[71] S. Kumar, R.K. Singh, Recovery of hydrocarbon liquid from waste high density polyethylene by thermal pyrolysis, Braz. J. Chem. Eng. 28 (2011) 659–667.
[72] J.M. Heikkinen, J.C. Hordijk, W.D. Jong, H. Spliethoff, Thermogravimetry as a tool to classify waste components to be used for energy generation, J. Anal. Appl. Pyrol. 71 (2004) 883–900.
[73] L. Chin, S. Yusup, A. Alshoaibi, P. Kannan, C. Srinivasakannan, S.A. Sulaiman, Kinetic studies of co-pyrolysis of rubber seed shell with high density polyethylene, Energy Convers. Manag. 87 (2014) 746–753.
[74] Ö. CEpeliÏOgUllar, A.E. Pütün, Thermal and kinetic behaviors of biomass and plastic wastes in co-pyrolysis, Energy Convers. Manag. 75 (2013) 263–270.
[75] S. Kim, Pyrolysis kinetics of waste PVC pipe, Waste Manag. 21 (2001) 609–616.
[76] J. Yu, L. Sun, C. Ma, Y. Qiao, H. Yao, Thermal degradation of PVC: a review, Waste Manag. 48 (2015) 300–314.
[77] B. Saha, A.K. Maiti, A.K. Ghoshal, Model-free method for isothermal and non-isothermal decomposition kinetics analysis of PET sample, Mol. Phys. 104 (2006) 2457–2464.
[78] R. Cherbański, K. Wróblewski, E. Molga, Pyrolysis of waste tyres-The effect of reaction kinetics on the results of thermogravimetric analysis, Chem. Process Eng. 38 (2017) 363–377.

[79] G. Lopez, J. Alvarez, M. Amutio, N.M. Mkhize, B. Danon, P.V.D. Gryp, et al., Waste truck-tyre processing by flash pyrolysis in a conical spouted bed reactor, Energy Convers. Manag. 142 (2017) 523–532.
[80] K.Y. Cheung, K.L. Lee, K.L. Lam, C.W. Lee, C.W. Hui, Integrated kinetics and heat flow modelling to optimise waste tyre pyrolysis at different heating rates, Fuel Process. Technol. 92 (2011) 856–863.
[81] K.L. Lam, A.O. Oyedun, K.Y. Cheung, K.L. Lee, C.W. Hui, Modelling pyrolysis with dynamic heating, Chem. Eng. Sci. 66 (2011) 6505–6514.
[82] E. Aylón, A. Fernándezcolino, R. Murillo, G. Grasa, M.V. Navarro, T. García, et al., Waste tyre pyrolysis: modelling of a moving bed reactor, Waste Manag. 30 (2010) 2530–2536.
[83] A. Oyedun, K.L. Lam, M. Fittkau, C.W. Hui, Optimisation of particle size in waste tyre pyrolysis, Fuel 95 (2012) 417–424.
[84] Y. Ding, B. Huang, K. Li, W. Du, K. Lu, Y. Zhang, Thermal interaction analysis of isolated hemicellulose and cellulose by kinetic parameters during biomass pyrolysis, Energy 195 (2020), 117010.
[85] Y. Ding, O.A. Ezekoye, S. Lu, C. Wang, Thermal degradation of beech wood with thermogravimetry/Fourier transform infrared analysis, Energy Convers. Manag. 120 (2016) 370–377.
[86] Y. Ding, C. Wang, M. Chaos, R. Chen, S. Lu, Estimation of beech pyrolysis kinetic parameters by Shuffled Complex Evolution, Bioresour. Technol. 200 (2016) 658–665.
[87] C. Branca, A. Albano, C. Di Blasi, Critical evaluation of global mechanisms of wood devolatilization, Thermochim. Acta 429 (2005) 133–141.
[88] J. Zhang, T. Chen, J. Wu, J. Wu, A novel Gaussian-DAEM-reaction model for the pyrolysis of cellulose, hemicellulose and lignin, RSC Adv. 4 (2014), 17513.
[89] H. Bockhorn, A. Hornung, U. Hornung, J. Weichmann, Kinetic study on the non-catalysed and catalysed degradation of polyamide 6 with isothermal and dynamic methods, Thermochim. Acta 337 (1999) 97–110.
[90] H. Hornung, S. Donner, M. Gernsbeck, A. Hornung, U. Hornung, Pyrolysis of polyamide 6 under catalytic conditions and its application to reutilization of carpets, J. Anal. Appl. Pyrol. 58–59 (2001) 79–94.
[91] P. Straka, J. Náhunková, Z. Brožová, Kinetics of copyrolysis of coal with polyamide 6, J. Anal. Appl. Pyrol. 71 (2004) 213–221.
[92] L. Jiao, G. Xu, Q. Wang, Q. Xu, J. Sun, Kinetics and volatile products of thermal degradation of building insulation materials, Thermochim. Acta 547 (2012) 120–125.
[93] L. Jiao, H. Xiao, Q. Wang, J. Sun, Thermal degradation characteristics of rigid polyurethane foam and the volatile products analysis with TG-FTIR-MS, Polym. Degrad. Stabil. 98 (2013) 2687–2696.
[94] H. Huang, J. Liu, H. Liu, F. Evrendilek, M. Buyukada, Pyrolysis of water hyacinth biomass parts: bioenergy, gas emissions, and by-products using TG-FTIR and Py-GC/MS analyses, Energy Convers. Manag. 207 (2020), 112552.
[95] J. Hu, Practical FTIR Spectra, Science Press, Beijing, China, 2011.
[96] Z. Ding, Z. Chen, J. Liu, F. Evrendilek, Y. He, W. Xie, Co-combustion, life-cycle circularity, and artificial intelligence-based multi-objective optimization of two plastics and textile dyeing sludge, J. Hazard Mater. 426 (2022), 128069.